Transportation Research Part C 105 (2019) 405–421

Contents lists available at ScienceDirect

Transportation Research Part C

journal homepage: www.elsevier.com/locate/trc

Corridor level cooperative trajectory optimization with connected and automated vehicles

Chunhui Yu[a], Yiheng Feng[b,*], Henry X. Liu[b,c], Wanjing Ma[a], Xiaoguang Yang[a]

[a] Key Laboratory of Road and Traffic Engineering of the Ministry of Education, Tongji University, 4800 Cao'an Road, Shanghai, PR China
[b] University of Michigan Transportation Research Institute (UMTRI), 2901 Baxter Rd, Ann Arbor, MI 48109, United States
[c] Department of Civil and Environmental Engineering, University of Michigan, 2320 G.G. Brown, 2350 Hayward Street, Ann Arbor, MI, United States

ARTICLE INFO

Keywords:
Connected and automated vehicle
Trajectory optimization and coordination
Corridor
Mixed-integer linear programming

ABSTRACT

Trajectory planning for connected and automated vehicles (CAVs) has been studied at both isolated intersections and multiple intersections under the fully CAV environment in the literature. However, most of the existing studies only model limited interactions of vehicle trajectories at the microscopic level, without considering the coordination between vehicle trajectories. This study proposes a mixed-integer linear programming (MILP) model to cooperatively optimize the trajectories of CAVs along a corridor for system optimality. The car-following and lane-changing behaviors of each vehicle along the entire path are optimized together. The trajectories of all vehicles along the corridor are coordinated for system optimality in terms of total vehicle delay. All vehicle movements (i.e., left-turning, through, and right-turning) are considered at each intersection. The ingress lanes are not associated with any specific movement and can be used for all vehicle movements, which provides much more flexibility. Vehicles are controlled to pass through intersections without traffic signals. Due to varying traffic conditions, the planning horizon is adaptively adjusted in the implementation procedure of the proposed model to find a balance between solution feasibility and computational burden. Numerical studies validate the advantages of the proposed CAV-based control over the coordinated fixed-time control at different demand levels in terms of vehicle delay and throughput. The analyses of the safety time gaps for collision avoidance within intersection areas show the promising benefits of traffic management under the fully CAV environment.

1. Introduction

Traffic control at intersections is crucial to ensure both safety and efficiency of urban transportation networks. Conventionally, priority rules (stop signs, roundabouts, right-before-left, etc.) and traffic signals are used to assign rights of way (ROW) and manage conflicting traffic streams. In terms of controlling intersections with traffic signals, there are three general approaches: fixed-time control, vehicle-actuated control, and adaptive control (Papageorgiou et al., 2003). All the approaches can be applied to either an isolated intersection, a corridor or a traffic network. Fixed-time control adopts signal timings optimized offline based on historical traffic data. Actuated and adaptive control adjust signal timings in real time to respond to varying traffic conditions with the aid of infrastructure-based vehicle detectors. Numerous studies have been dedicated to these research areas to improve the efficiency of traffic control (Allsop, 1976; Han and Gayah, 2015; Han et al., 2014; Heydecker, 1992; Little et al., 1981; Liu and Smith, 2015;

* Corresponding author.
E-mail address: yhfeng@umich.edu (Y. Feng).

https://doi.org/10.1016/j.trc.2019.06.002
Received 6 November 2018; Received in revised form 5 June 2019; Accepted 5 June 2019

Memoli et al., 2017; Webster, 1958).

Recent advances in connected and automated vehicle (CAV) technologies render it possible to communicate between vehicles (V2V) and between vehicles and infrastructure (V2I), which provides a new source of data for traffic management. One research direction is to incorporate real-time vehicle trajectory information (e.g., speeds and locations) into signal optimization with infrastructure-based detector data. Signal parameters such as phase sequence and phase duration are optimized for individual intersections (Feng et al., 2015; Gradinescu et al., 2007; Ilgin Guler et al., 2014; Liang et al., 2018; Yang et al., 2018) and multiple intersections (He et al., 2012; Yang et al., 2017). Another direction is to optimize vehicle trajectories with the objectives to reduce fuel/energy consumption, emission, as well as vehicle delay, given fixed signal timings. Naturally, optimal control models or feedback control models are formulated with vehicle speeds or acceleration rates as the control variables (Kamal et al., 2013; Ubiergo and Jin, 2016; Wan et al., 2016; Wang et al., 2014a; Wang et al., 2014b). In order to solve the models more efficiently, approximation is often adopted to either discretize the models (e.g., time discretization) or reduce the number of parameters (e.g., trajectory segmentation) (He et al., 2015; Kamalanathsharma and Rakha, 2013; Miyatake et al., 2011). Recent studies have proposed to integrate traffic signal control and vehicle trajectory control in a unified framework. To this end, enumeration of feasible signal plans and trajectory segmentation were combined in Li et al. (2014). Feng et al. (2018) combined an optimal control model for trajectory planning and a dynamic programming model for signal optimization into a two-stage optimization model. Instead of applying a two-stage optimization process, Yu et al. (2018) proposed a mixed-integer linear programming (MILP) model to simultaneously optimize phase sequences, green start and duration of each phase, cycle lengths together with vehicle lane-changing behaviors and vehicle arrival times. Guo et al. (2019b) proposed a two-step approach to optimize vehicle trajectories and signal timings based on a DP-SH (dynamic programming with shooting heuristic as a subroutine) algorithm for efficiency.

Assuming a 100% CAV environment, the concept of “signal-free” intersections has been proposed (Dresner and Stone, 2008), in which vehicles cooperate with each other and pass through intersections without physical traffic signals. One prevailing category of such studies are based on certain reservation mechanisms. Approaching vehicles send requests to the intersection controller to reserve spaces and time slots within the intersection area. Reservation requests can be accepted or rejected based on their conflicts with previous reservations. The service sequence of vehicles is usually determined by rule-based policies such as “first-come, first-served” (FCFS) strategy (Au and Stone, 2010; Dresner and Stone, 2008; Li et al., 2013), auction strategy (Carlino et al., 2013), priority strategy (Alonso et al., 2011) and platooning strategy (Tachet et al., 2016). However, the optimality of the existing reservation-based approaches is not guaranteed because of its rule-based nature. Optimization-based models are also proposed. Lee and Park (2012) proposed a constrained nonlinear optimization model to optimize vehicle acceleration/deceleration rates. The objective was minimization of trajectory overlap with the focus on safety. On the other hand, Zohdy and Rakha (2016) focused more on efficiency and presented a constrained nonlinear optimization model to optimize vehicle arrival times at intersections with the objective of delay minimization. Xu et al. (2018) proposed a distributed conflict-free cooperation method. Approaching vehicles from different traffic movements were projected into a virtual lane. A conflict-free geometry topology was then introduced with the consideration of the conflict relationship of involved vehicles. Mirheli et al. (2019) proposed a vehicle-level mixed-integer non-linear programming model for cooperative trajectory planning in a distributed way. Vehicle-level solutions were pushed towards the global optimality. Li et al. (2019) mathematically formulated 3D CAV trajectories in the combined temporal-spatial domains. Priority-based and Discrete Forward-Rolling Optimal Control (DFROC) algorithms were developed for CAV management at isolated intersections.

Besides isolated intersections, “signal-free” CAV management at multiple intersections is explored as well. Both the reservation- and the optimization-based approaches have been investigated. Hausknecht et al. (2011) and Levin et al. (2017) combined vehicle routing at the macroscopic level and the reservation-based control at the microscopic level. However, neither vehicle trajectory coordination nor lane-changing behaviors were taken into consideration. Giridhar and Kumar (2006) discretized space and time to optimize vehicle movements at each time step in a traffic network, which was modeled as a scheduling problem. Vehicles were assumed to move at a constant speed or be stationary. Zhu and Ukkusuri (2015) derived a lane-based traffic flow model from the cell transmission model and then proposed a linear programming formulation for CAV management at the network level. However, traffic flow propagation was used to model vehicles passing through the intersection. Interactions of individual vehicle trajectories were not taken into consideration.

Notwithstanding the abundant studies, it is noted that most related studies only apply to isolated intersections (Guo et al., 2019a). Moreover, the studies on multiple intersections fail to take into consideration microscopic trajectory interactions or trajectory coordination, which is the key to CAV trajectory planning. This paper takes a further step and studies the trajectory planning for CAVs along a “signal-free” corridor in a fully CAV environment. An MILP model is formulated to cooperatively optimize the trajectories of all vehicles in a corridor. As CAV trajectories are observable and controllable, they are coordinated to achieve system optimality in terms of vehicle delay. Microscopic interactions of vehicle trajectories on road segments (i.e., car-following behaviors and lane-changing behaviors) as well as within intersections (i.e., collision avoidance) are modeled explicitly. All different vehicle movements including left-turning, through, and right-turning traffic are considered. Each ingress lane is not associated with any specific vehicle movement and can be used for all vehicle movements, which provides much more flexibility compared to previous studies. To balance the solution feasibility and the computational complexity, the planning horizon is adaptively adjusted in the implementation procedure.

The remainder of this paper is structured as follows. Section 2 presents the problem. Section 3 builds the MILP model to optimize and coordinate vehicle trajectories along a corridor. Section 4 presents the implementation procedure of the proposed model with varying traffic conditions, which adaptively adjusts the planning horizon to improve computational efficiency. Numerical studies are conducted in Section 5. Finally, conclusions and recommendations are delivered in Section 6.

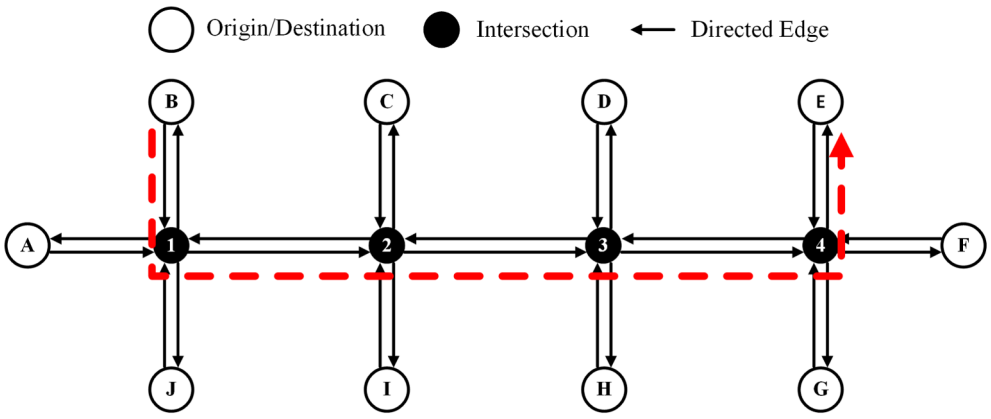

Fig. 1. A corridor with four intersections.

2. Problem description

Fig. 1 shows a corridor with four intersections in a macroscopic view as an example to describe the problem. Intersections and origins/destinations are shown as nodes. Roadways between intersections or origins/destinations are edges, which are directed. The red dash line is an exemplary path, which is a sequence of directed edges from original B to destination E, traversing four intersections. Fig. 2 shows the microscopic view of one intersection in the corridor. Each edge e along a path consists of two parts at the microscopic level, a link and all available connectors departing from the link. A link is defined as the roadway between two intersections or between an intersection and an origin/destination. A connector is defined as the roadway within an intersection, which connects two different links.

Take vehicle ω in Fig. 2 as an example. Assume its path p^ω is the red dash line in Fig. 1. The vehicle is traveling between intersection 3 and intersection 4 and wants to make a left turn at intersection 4. Then the edge where vehicle ω is traveling consists of the highlighted link and all connectors ahead, which include two for left-turning traffic, three for through traffic and two for right-turning traffic. Vehicles are allowed to make lane changes when they are far away from the intersection. But lane changing is forbidden when they are too close to the intersection, which is a common practice in real road networks. The area in which lane changing is forbidden is denoted as l_e in the figure. If $l_e = 0$, vehicles are not allowed to change lanes only within the intersection area. There are three main types of decision variables for each vehicle ω on each edge e along path p^ω. $x_e^\omega(t)$ is the distance between vehicle ω and the stop bar on edge e at time step t. $x_e^\omega(t) \geqslant 0$ before vehicle ω passes the stop bar on edge e at time step t. $x_e^\omega(t) < 0$, otherwise. In that case, $\|x_e^\omega(t)\|$ is the traveled distance in a connector after vehicle ω passes the stop bar. $\delta_k^\omega(t)$ is the lane choice of vehicle ω at time step t. $\delta_k^\omega(t) = 1$ if vehicle ω is in lane k at time step t. $\delta_k^\omega(t) = 0$, otherwise. $\underline{t}_e^\omega$ and $\bar{t}_e^\omega$ are the time points of entering edge e and leaving the link of edge e, respectively. $\underline{t}_e^\omega$ and $\bar{t}_e^\omega$ are continuous. The trajectory of vehicle ω is obtained after $x_e^\omega(t)$, $\underline{t}_e^\omega$, and $\bar{t}_e^\omega$ are determined for each edge e on path p^ω and $\delta_k^\omega(t)$ is determined for each lane k in the link of each edge e.

Note that there is no lane allocation at the intersection. That means, a vehicle can use any lane to pass through the intersection provided connectors exist for its movement. For example, vehicle ω can use the left two lanes to make a left turn. In this example, vehicle ω may have collisions with both through vehicle ω_2 in a different link and through vehicle ω_1 in the same link. This setup may increase the number of conflict points within the intersection, but is more flexible in lane assignment which can increase the intersection capacity significantly.

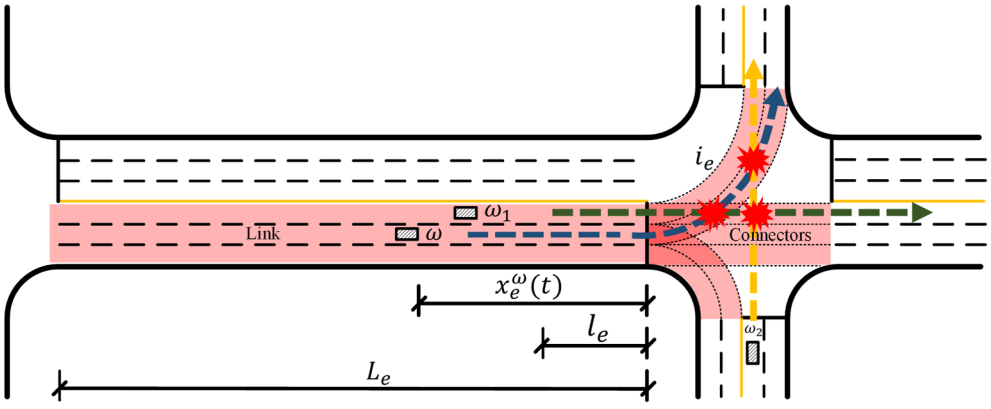

Fig. 2. A microscopic view of an intersection.

Given the geometric layout of a corridor and the vehicles in the corridor, the objective of this study is to cooperatively optimize the trajectories of all vehicles for total delay minimization. Both longitudinal locations of vehicles along their paths and lateral lane-changing behaviors are modeled explicitly. To simplify the formulation, the following assumptions are made:

- All vehicles are CAVs and can be controlled by a centralized controller without communication delay.
- The path of a vehicle is generated when the vehicle enters the corridor and it will not change afterwards.
- No lane-changing behaviors are allowed within intersection areas.
- Vehicles can change lanes instantly in the link of each edge.
- Vehicle dynamics are captured by the first order model, the same assumption as in Newell's car-following model (Newell, 2002). It does not mean vehicles follow Newell's car-following model because they are supposed to follow planned trajectories. But the acceleration and deceleration processes are not modeled. And
- The speed of a vehicle within an intersection area is determined by its movement. Different movements have different speeds due to the turning radius. But the vehicle keeps a constant speed in the connectors.

Some assumptions may seem unrealistic from the perspective of the current technologies. For example, the realization of the fully CAV environment is far away; the centralized control approach may raise computational burden and communication delays; and the transition of car-following and lane-changing behaviors is not considered and thus over-simplifies vehicle dynamics. However, this study aims to provide theoretical upper bound solutions in terms of system optimality that we strive to achieve with the advances of CAV technologies. Of course the actual benefits will be less when these assumptions are relaxed. Furthermore, this study serves as the start to take into consideration the microscopic interactions and coordination of vehicle trajectories for CAV management at multiple intersections. Therefore, the proposed model in this paper provides preliminary and important insights on the benefits of deploying CAVs in the future.

3. Problem formulations

This section presents the MILP model based on discrete time to cooperatively optimize vehicle trajectories. The longitudinal location and the lane changing behaviors along the path are optimized for each vehicle jointly. The objective function and constraints are presented in the following sub-sections. Before the formulation, main notations applied hereafter are summarized in the Table 1.

3.1. Constraints

Decision variable related constraints, vehicle movement related constraints, and safety related constraints are introduced in this section. The decision variables are constrained by variable domains and the boundary conditions at the start and the end of the planning horizon. The vehicle movement constraints deal with vehicle dynamics and vehicle driving behaviors when entering an edge, passing a stop bar, and changing lanes. The safety constraints guarantee the safety gaps between vehicles on the same edge and on adjacent edges (to avoid spillbacks) as well as the collision avoidance within intersection areas.

3.1.1. Domains of decision variables

The three main types of the decision variables are defined for each vehicle ω, which include $x_e^\omega(t)$ (i.e., location on edge e at time step t), $\delta_k^\omega(t)$ (indicating if in lane k at time step t), and $\underline{t}_e^\omega$ and $\bar{t}_e^\omega$ (time points of entering and leaving the link of edge e).

Denote e_0^ω as the currently occupied edge by vehicle ω. If vehicle ω is in the link of edge e_0^ω, then $\underline{t}_e^\omega$ and $\bar{t}_e^\omega$ are constrained by

$$\underline{t}_e^\omega = \underline{t}_0^\omega \leq 0,\ \forall\ e \in p^\omega,\ e = e_0^\omega;\omega \in \mathbf{\Omega} \tag{1}$$

$$0 \leqslant \bar{t}_e^\omega \leqslant T{\cdot}\Delta t,\ \forall\ e \in p^\omega,\ e = e_0^\omega;\omega \in \mathbf{\Omega} \tag{2}$$

where $\underline{t}_0^\omega$ is the time of entering edge e_0^ω; $\mathbf{\Omega}$ is the set of vehicles in the corridor. $\underline{t}_e^\omega$ is a relative value to the current time, which is non-positive. If vehicle ω is in a connector of edge e_0^ω, then the following constraint of $\bar{t}_e^\omega$ is used instead of Eq. (2):

$$\bar{t}_e^\omega = \bar{t}_0^\omega \leq 0,\ \forall\ e \in p^\omega,\ e = e_0^\omega;\omega \in \mathbf{\Omega} \tag{3}$$

where $\bar{t}_0^\omega$ is the time of passing the stop bar on edge e_0^ω and is a relative value to the current time.

For other edges to be traveled along the path (i.e., $e \in p^\omega$, $e \neq e_0^\omega$), t_e^ω and $\bar{t}_e^\omega$ are non-negative and bounded by the planning horizon $T{\cdot}\Delta t$:

$$0 \leqslant \underline{t}_e^\omega \leqslant T{\cdot}\Delta t,\ \forall\ e \in p^\omega,\ e \neq e_0^\omega;\omega \in \mathbf{\Omega} \tag{4}$$

$$0 \leqslant \bar{t}_e^\omega \leqslant T{\cdot}\Delta t,\ \forall\ e \in p^\omega,\ e \neq e_0^\omega;\omega \in \mathbf{\Omega} \tag{5}$$

Further, vehicle speeds on an edge are bounded, which means

$$\bar{t}_e^\omega \geqslant \underline{t}_e^\omega,\ \forall\ e \in p^\omega;\omega \in \mathbf{\Omega} \tag{6}$$

Before vehicle ω enters edge e on its path p^ω, $x_e^\omega(t)$ is defined as the length of the link of edge e (i.e., L_e) for continuity:

$$\mathrm{M}\underline{\mu}_e^\omega(t) \geqslant x_e^\omega(t) - L_e \geqslant -\mathrm{M}\underline{\mu}_e^\omega(t),\ \forall\ t = 0,\ ...,T;e \in p^\omega;\omega \in \mathbf{\Omega} \tag{7}$$

Table 1
Notations.

General notations	
M:	A sufficiently large number
$\mathbf{\Omega}$:	Set of vehicles in the corridor; each vehicle is denoted as ω
$\mathbf{\Omega}_\omega$:	Set of vehicles whose paths overlap with the path of vehicle ω
p^ω:	Path of vehicle ω
$\underline{p}^\omega/\underline{p}^\omega_+$:	First/last edge of path p^ω
e:	Edge on a path, which consists of one link and all departing connectors
e^ω_+/e^ω_-:	Succeeding/preceding edge of edge e on path p^ω of vehicle ω
e^ω_0:	Edge on which vehicle ω is traveling at current time step
i_e:	Downstream intersection of edge e
$\mathbf{K}_e$:	Set of lanes in the link of edge e; each lane is denoted as k
$\mathbf{K}^\omega_e$:	Set of candidate lanes for vehicle ω to pass the stop bar on edge e
k^ω_+/k^ω_-:	Succeeding/preceding lane of lane k on the path of vehicle ω; that is, lane k^ω_+/k^ω_- is connected from/to lane k by a connector
Parameters	
Δt:	Length of time step, s
t_0:	Current time step when vehicle trajectories are optimized
T:	Planning horizon
T_0:	Initial value of T in the adaptive algorithm for planning horizon
ΔT:	Step length for T in the adaptive algorithm for planning horizon
L_e:	Length of the link of edge e, m
l_e:	Control area where no lane changing is allowed on edge e, m
l^ω_k:	Length of the connector from lane k on the path of vehicle ω, m
v^ω_k:	Speed of vehicle ω in the connector from lane k on the path of vehicle ω, m/s
$\bar{v}^\omega_e$:	Maximum speed for vehicle ω in the link of edge e, m/s
$tt^{\omega,k}_{\omega',k'}$:	Travel time for vehicle ω in lane k from the stop bar to the conflict point with vehicle ω' in lane k', s
st:	Safety time gap between two vehicles passing the conflict point consecutively, s
x^ω_0:	Distance from vehicle ω to the stop bar on the current edge at current time step, m
δ^ω_{0k}:	1, if vehicle ω is in lane k on the current edge at current time step; 0, otherwise
$\underline{t}^\omega_0$:	Recorded time point for vehicle ω entering the current edge, which is a relative value to the current time, s
$\bar{t}^\omega_0$:	Recorded time point for vehicle ω passing the stop bar on the current edge when the vehicle is in a connector, which is a relative value to the current time, s
d:	Space displacement in Newell's car-following model, m
τ:	Time displacement in Newell's car-following model, s
w_1/w_2:	Weighting parameter in the objective function
Decision variables	
$x^\omega_e(t)$:	Distance from vehicle ω to the stop bar on edge e at time step t, m
$\delta^\omega_k(t)$:	1, if vehicle ω is in lane k at time step t; 0, otherwise
$\underline{t}^\omega_e/\bar{t}^\omega_e$:	Time point of entering/leaving the link of edge e for vehicle ω, s
Auxiliary variables	
$\underline{\mu}^\omega_e(t)$:	1, if $t\cdot\Delta t \geqslant \underline{t}^\omega_e$ (i.e., vehicle ω has visited edge e by time step t); 0, otherwise
$\mu^\omega_e(t)$:	1, if $t\cdot\Delta t \geqslant \bar{t}^\omega_e$ (i.e., vehicle ω has passed the stop bar on edge e by time step t); 0, otherwise
$\chi^{\omega,\omega'}_e(t)$:	0, if vehicle ω and vehicle ω' are in the same lane on edge e at time step t; 2, otherwise
$\rho^{\omega,\omega'}_e(t)$:	0, if safety distance between vehicles ω and ω' is applied on edge e at time step t; 1, otherwise
v^ω_e:	Travelling speed within the intersection area for vehicle ω from edge e, m/s
$\gamma^{\omega,e}_{\omega',e'}$:	0, if vehicle ω' from edge e' follows vehicle ω from edge e to pass their conflict point; 1, otherwise
$\pi^{\omega,e}_{\omega',e'}$:	Clearance time between departure times from stop bars if vehicle ω' from edge e' follows vehicle ω from edge e to pass the same conflict point, s
$\zeta^{\omega,\omega'}_e(t)$:	1, if vehicle ω follows vehicle ω' in a lane on edge e at time step t; 0, otherwise
$\xi^{\omega,\omega'}_e$:	1, if vehicle ω follows vehicle ω' to pass the stop bar on edge e; 0, otherwise
$\tilde{\zeta}^{\omega,\omega'}_e(t)$:	0, if vehicle ω' is on edge e and vehicle ω is in a connector of the preceding edge e^ω_- at time step t

where $\underline{\mu}^\omega_e(t)$ is an auxiliary binary variable. $\underline{\mu}^\omega_e(t) = 1$ if vehicle ω has entered edge e at time step t;$\underline{\mu}^\omega_e(t) = 0$, otherwise. Eq. (7) guarantees that $x^\omega_e(t) = L_e$ when $\underline{\mu}^\omega_e(t) = 0$. $x^\omega_e(t)$ will be constrained in the following Eqs. (8) and (9) when $\underline{\mu}^\omega_e(t) = 1$.

When vehicle ω travels in the link of edge e, $x^\omega_e(t)$ is bounded by

$$L_e \geqslant x^\omega_e(t) \geqslant -\mathrm{M}(1 - \underline{\mu}^\omega_e(t) + \bar{\mu}^\omega_e(t)),\ \forall\ t = 0,\ ...,T;e \in p^\omega;\omega \in \mathbf{\Omega} \tag{8}$$

where $\bar{\mu}^\omega_e(t)$ is an auxiliary binary variable. $\bar{\mu}^\omega_e(t) = 1$ if vehicle ω has passed the stop bar on edge e at time step t;$\bar{\mu}^\omega_e(t) = 0$, otherwise. Eq. (8) guarantees that $L_e \geqslant x^\omega_e(t) \geq 0$ when $\underline{\mu}^\omega_e(t) = 1$ and $\bar{\mu}^\omega_e(t) = 0$.

After vehicle ω passes the stop bar on edge e (i.e., $\underline{\mu}^\omega_e(t) = 1$ and $\bar{\mu}^\omega_e(t) = 1$), $x^\omega_e(t)$ is defined as a negative value, whose absolute value indicates the traveled distance in a connector after passing the stop bar:

$$\mathrm{M}(1-\bar{\mu}_e^{\omega}(t)) \geqslant x_e^{\omega}(t) + v_e^{\omega}(t\cdot\Delta t - \bar{t}_e^{\omega}) \geqslant -\mathrm{M}(1-\bar{\mu}_e^{\omega}(t)),\ \forall\ t=0,\ ...,T; e\in p^{\omega}; \omega\in\mathbf{\Omega} \tag{9}$$

where v_e^{ω} is the speed of vehicle ω in a connector of edge e. Note that only $\bar{\mu}_e^{\omega}(t)$ is used in Eq. (9). Because $\underline{\mu}_e^{\omega}(t)$ must be one when $\bar{\mu}_e^{\omega}(t)=1$ according to their definitions. Eq. (9) indicates that $x_e^{\omega}(t) = -v_e^{\omega}(t\cdot\Delta t - \bar{t}_e^{\omega})$ when $\bar{\mu}_e^{\omega}(t)=1$. v_e^{ω} is determined by the choice of lanes from which vehicle ω enters the intersection area:

$$v_e^{\omega} = \sum_{k\in\mathbf{K}_e^{\omega}} \delta_k^{\omega}(T) v_k^{\omega},\ \forall\ e\in p^{\omega}; \omega\in\mathbf{\Omega} \tag{10}$$

where v_k^{ω} is the speed of vehicle ω in the connector departing from lane k on its path, which is a determined parameter based on the turning movement of vehicle ω; $\mathbf{K}_e^{\omega}$ is the set of the lanes vehicle ω can use to pass the stop bar on edge e. For example, the left-turning vehicle ω in Fig. 2 can only use the left two lanes for its movement. Eq. (10) guarantees that $v_e^{\omega} = v_k^{\omega}$ when vehicle ω passes through the intersection from lane k (i.e., $\delta_k^{\omega}(T)=1$). Note that the final time step T is used in Eq. (10) because $\delta_k^{\omega}(t)$ will be constrained to be the same after vehicle ω passes the stop bar in the following constraint Eq. (28).

3.1.2. Boundary conditions

For the currently occupied edge e_0^{ω}, $x_e^{\omega}(0)$ is determined by the current location of vehicle ω:

$$x_e^{\omega}(0) = x_0^{\omega},\ \forall\ e\in p^{\omega},\ e=e_0^{\omega}; \omega\in\mathbf{\Omega} \tag{11}$$

For other edges to be traveled along the path (i.e., $e\in p^{\omega}$, $e\neq e_0^{\omega}$), $x_e^{\omega}(0)$ is set as L_e:

$$x_e^{\omega}(0) = L_e,\ \forall\ e\in p^{\omega},\ e\neq e_0^{\omega}; \omega\in\mathbf{\Omega} \tag{12}$$

Similarly, $\delta_k^{\omega}(0)$ for the lanes on edge e_0^{ω} is determined by the current lane choice of vehicle ω:

$$\delta_k^{\omega}(0) = \delta_{0k}^{\omega},\ \forall\ k\in\mathbf{K}_e; e\in p^{\omega},\ e=e_0^{\omega}; \omega\in\mathbf{\Omega} \tag{13}$$

where $\mathbf{K}_e$ is the set of lanes in the link of edge e.

At the end of the planning horizon, every vehicle ω is supposed to have passed the stop bar on the last edge on its path:

$$x_{p_+^{\omega}}^{\omega}(T) < 0,\ \forall\ \omega\in\mathbf{\Omega} \tag{14}$$

where p_+^{ω} is the last edge on path p^{ω}.

3.1.3. Vehicle dynamics

Vehicles are not allowed to move backward on edges for safety concerns. That is, $x_e^{\omega}(t+1)$ should not be larger than $x_e^{\omega}(t)$ as shown in Fig. 3:

$$x_e^{\omega}(t+1) \leqslant x_e^{\omega}(t),\ \forall\ t=0,\ ...,T-1; e\in p^{\omega}; \omega\in\mathbf{\Omega} \tag{15}$$

If vehicle ω enters edge e during time step $t+1$ (i.e., $\underline{\mu}_e^{\omega}(t)=0$ and $\underline{\mu}_e^{\omega}(t+1)=1$) as shown in Fig. 4, the traveled distance on edge e during this time step is constrained by the maximum speed $\bar{v}_e^{\omega}$ on edge e:

$$L_e - x_e^{\omega}(t+1) \leqslant \bar{v}_e^{\omega}((t+1)\Delta t - \underline{t}_e^{\omega}) + \mathrm{M}(1+\underline{\mu}_e^{\omega}(t) - \underline{\mu}_e^{\omega}(t+1)),\ \forall\ t=0,\ ...,T-1; e\in p^{\omega}; \omega\in\mathbf{\Omega} \tag{16}$$

Eq. (16) is effective only when $\underline{\mu}_e^{\omega}(t)=0$ and $\underline{\mu}_e^{\omega}(t+1)=1$.

Similar constraints are given when vehicle ω travels in the link of edge e (i.e., $\underline{\mu}_e^{\omega}(t)=1$ and $\bar{\mu}_e^{\omega}(t+1)=0$) as show in Fig. 3:

$$x_e^{\omega}(t) - x_e^{\omega}(t+1) \leqslant \bar{v}_e^{\omega}\Delta t + \mathrm{M}(1-\underline{\mu}_e^{\omega}(t) + \bar{\mu}_e^{\omega}(t+1)),\ \forall\ t=0,\ ...,T-1; e\in p^{\omega}; \omega\in\mathbf{\Omega} \tag{17}$$

Eq. (17) is effective only when $\underline{\mu}_e^{\omega}(t)=1$ and $\bar{\mu}_e^{\omega}(t+1)=0$.

If vehicle ω passes the stop bar on edge e during time step $t+1$ (i.e., $\bar{\mu}_e^{\omega}(t)=0$ and $\bar{\mu}_e^{\omega}(t+1)=1$) as shown in Fig. 5, $x_e^{\omega}(t)$ is

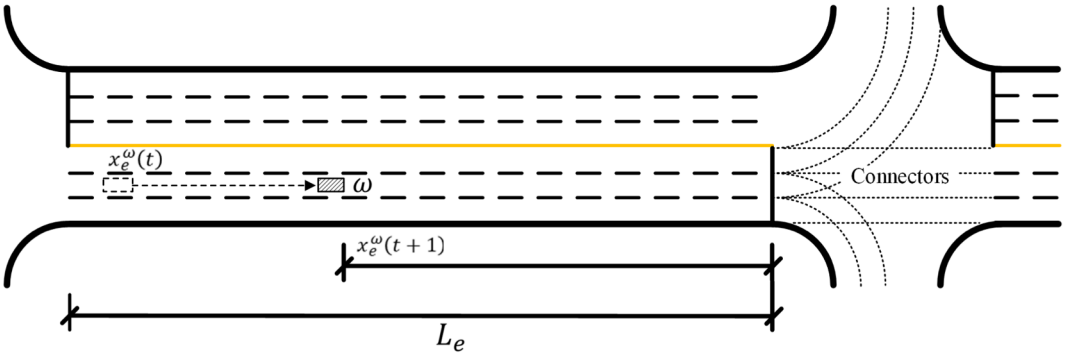

Fig. 3. Traveling on edge e during time step $t+1$.

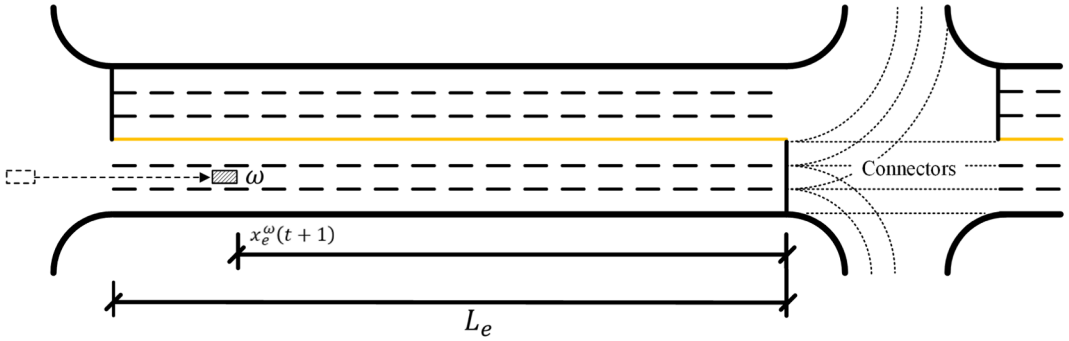

Fig. 4. Entering edge e during time step $t + 1$.

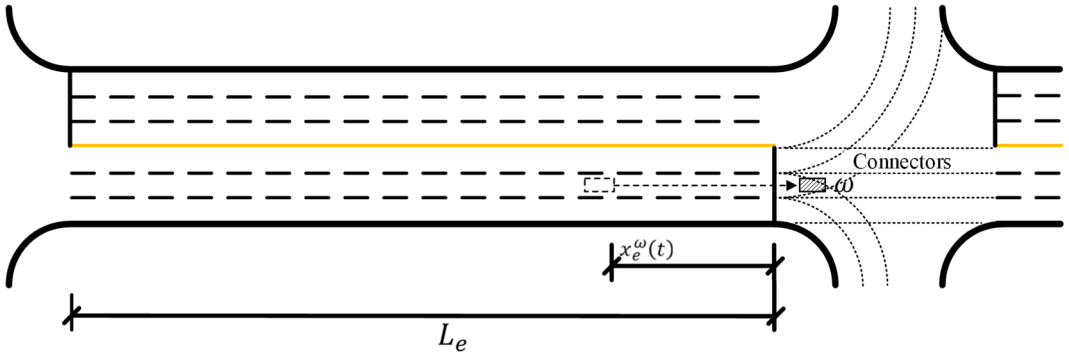

Fig. 5. Passing the stop bar on edge e during time step $t + 1$.

constrained by the maximum speed $\bar{v}_e^\omega$:

$$x_e^\omega(t) \leqslant \bar{v}_e^\omega(\bar{t}_e^\omega - t\cdot\Delta t) + \mathrm{M}(1 + \bar{\mu}_e^\omega(t) - \bar{\mu}_e^\omega(t+1)),\ \forall\ t = 0,\ ..., T-1; e \in p^\omega; \omega \in \mathbf{\Omega} \tag{18}$$

Eq. (18) is effective only when $\bar{\mu}_e^\omega(t) = 0$ and $\bar{\mu}_e^\omega(t+1) = 1$. In that case, $x_e^\omega(t+1)$ is determined in Eq. (9).

At any time step t within the planning horizon, vehicle ω can only occupy one lane in the link of each edge e:

$$\sum_{k\in\mathbf{K}_e} \delta_k^\omega(t) = 1,\ \forall\ t = 0,\ ..., T; e \in p^\omega; \omega \in \mathbf{\Omega} \tag{19}$$

It is assumed that vehicle ω can only change one lane within one time step. That is, if vehicle ω is in lane k at time step t ($\delta_k^\omega(t) = 1$), then it can only take its current and adjacent lanes at time step $t + 1$:

$$1 - \delta_k^\omega(t) \geqslant \delta_{k'}^\omega(t+1) \geqslant \delta_k^\omega(t) - 1,\ \forall\ t = 0,\ ..., T-1; k, k' \in \mathbf{K}_e,\ |k' - k| \geq 2; e \in p^\omega; \omega \in \mathbf{\Omega} \tag{20}$$

Although lane changing takes time in the reality, it is not difficult to apply such constraints to the proposed model in this paper.

If vehicle ω is stopped during time step $t + 1$ (i.e., $x_e^\omega(t) = x_e^\omega(t+1)$), then it cannot change lanes and should remain in its current lane (i.e., $\delta_k^\omega(t+1) = \delta_k^\omega(t)$):

$$\begin{aligned}&\mathrm{M}(x_e^\omega(t) - x_e^\omega(t+1)) \geqslant \delta_k^\omega(t+1) - \delta_k^\omega(t) \geqslant -\mathrm{M}(x_e^\omega(t) - x_e^\omega(t+1))\\ &\forall\ t = 0, ..., T-1; k \in \mathbf{K}_e; e \in p^\omega; \omega \in \mathbf{\Omega}\end{aligned} \tag{21}$$

Although the first order vehicle dynamics model is used, the proposed framework in this paper can also accommodate a higher order dynamics model. For example, if a second order model is applied, then the constraints of the maximum acceleration and deceleration rates should be included additionally. However, in that case, the assumption that the speed of a vehicle within an intersection area is determined by its movement will not hold. The proposed optimization model is no longer linear or convex. The solving algorithm could be another challenge. We leave the work of modeling higher order vehicle dynamics for future research.

3.1.4. Entering edges

Denote e_+^ω as the succeeding edge of edge e on path p^ω of vehicle ω. The time when vehicle ω enters edge e_+^ω is determined by time $\bar{t}_e^\omega$ when ω passes the stop bar on edge e and the lane choice at time $\bar{t}_e^\omega$ as shown in Fig. 6:

$$\underline{t}_{e_+^\omega}^\omega = \bar{t}_e^\omega + \sum_{k\in\mathbf{K}_e^\omega} \delta_k^\omega(T)\cdot\frac{l_k^\omega}{v_k^\omega},\ \forall\ e \in p^\omega,\ e \neq p_+^\omega; \omega \in \mathbf{\Omega} \tag{22}$$

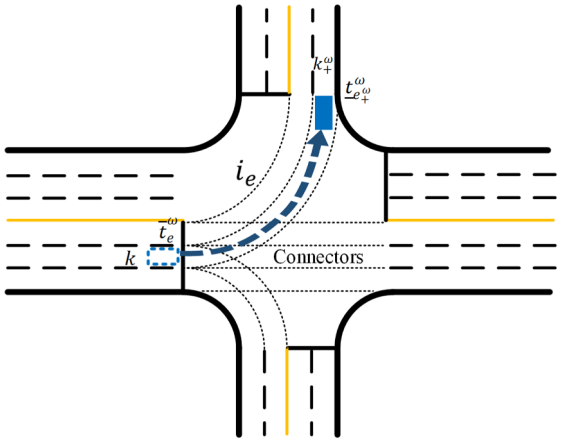

Fig. 6. Entering the succeeding edge.

where l_k^ω/v_k^ω is the travel time of vehicle ω in the connector departing from lane k, which is a constant. If vehicle ω leaves edge e in lane k, then $\delta_k^\omega(T)=1$. According to Eq. (22), $\underline{t}_{e_+^\omega}^\omega = \bar{t}_e^\omega + \frac{l_k^\omega}{v_k^\omega}$.

Denote k_+^ω as the succeeding lane on edge e_+^ω of lane k on edge e along path p^ω of vehicle ω. The lane in which vehicle ω enters edge e_+^ω is determined by the choice of the lane when vehicle ω passes the stop bar on edge e as shown in Fig. 6:

$$\delta_{k_+^\omega}^\omega(0)=\delta_k^\omega(T),\ \forall\ k\in\mathbf{K}_e^\omega; e\in p^\omega,\ e\ \neq\ p_+^\omega;\omega\in\mathbf{\Omega} \tag{23}$$

If vehicle ω leaves edge e in lane k, then $\delta_k^\omega(T)=1$. According to Eq. (23), $\delta_{k_+^\omega}^\omega(0)=1$. If vehicle ω enters the succeeding edge e_+^ω during time step $t'+1$ (i.e., $\underline{\mu}_{e_+^\omega}^\omega(t')=0$ and $\underline{\mu}_{e_+^\omega}^\omega(t'+1)=1$), then $x_{e_+^\omega}^\omega(t)=L_{e_+^\omega}$ for time step $t\leqslant t'$ according to Eq. (7). Further, $\delta_{k_+^\omega}^\omega(t')=\delta_{k_+^\omega}^\omega(t'-1)=\cdots=\delta_{k_+^\omega}^\omega(0)=1$ according to Eq. (21). For safety concerns, vehicles are not permitted to change lanes in connectors within intersection areas until they travel into succeeding edges, i.e., $\delta_{k_+^\omega}^\omega(t')=\delta_{k_+^\omega}^\omega(t'+1)=1$. That is, vehicle ω enters the succeeding edge e_+^ω in lane k_+^ω. This is specified by

$$\begin{aligned}&-(1+\underline{\mu}_e^\omega(t)-\underline{\mu}_e^\omega(t+1))\leqslant\delta_k^\omega(t)-\delta_k^\omega(t+1)\leq 1+\underline{\mu}_e^\omega(t)-\underline{\mu}_e^\omega(t+1)\\&\forall\ t=0,\ldots,T-1; k\in\mathbf{K}_e^\omega; e\in p^\omega;\omega\in\mathbf{\Omega}\end{aligned} \tag{24}$$

Eq. (24) guarantees that $\delta_k^\omega(t)=\delta_k^\omega(t+1)$ when $\underline{\mu}_e^\omega(t)=0$ and $\underline{\mu}_e^\omega(t+1)=1$.

$\underline{\mu}_e^\omega(t)$ is an auxiliary variable for the convenience of modeling. It is related to $\underline{t}_e^\omega$ in the following Eq. (25):

$$\mathrm{M}\underline{\mu}_e^\omega(t)\geqslant t\cdot\Delta t-\underline{t}_e^\omega\geqslant-\mathrm{M}(1-\underline{\mu}_e^\omega(t)),\ \forall\ t=0,\ \ldots,T; e\in p^\omega;\omega\in\mathbf{\Omega} \tag{25}$$

Eq. (25) indicates that $\underline{\mu}_e^\omega(t)=1$ if $t\cdot\Delta t>\underline{t}_e^\omega$ (i.e., vehicle ω has visited edge e by time step t) and $\underline{\mu}_e^\omega(t)=0$, otherwise.

3.1.5. Passing stop bars on edges

If vehicle ω passes the stop bar on edge e during time step $t+1$ (i.e., $\bar{\mu}_e^\omega(t)=0$ and $\bar{\mu}_e^\omega(t+1)=1$) as shown in Fig. 5, then $x_e^\omega(t)\geq 0$ and $x_e^\omega(t+1)<0$. The above Eqs. (7) and (8) guarantee that $x_e^\omega(t)\geq 0$ when $\bar{\mu}_e^\omega(t)=0$ (i.e., vehicle ω has not passed the stop bar on edge e by time step t). Eq. (9) guarantees that $x_e^\omega(t+1)<0$ when $\bar{\mu}_e^\omega(t+1)=1$.

When vehicle ω passes the stop bar on edge e, only one lane in $\mathbf{K}_e^\omega$ can be used:

$$\sum_{k\in\mathbf{K}_e^\omega}\delta_k^\omega(T)=1,\ \forall\ e\in p^\omega;\omega\in\mathbf{\Omega} \tag{26}$$

$\bar{\mu}_e^\omega(t)$ is auxiliary variable for the convenience of modeling. It is related to $\bar{t}_e^\omega$ in the following Eq. (27):

$$\mathrm{M}\bar{\mu}_e^\omega(t)\geqslant t\cdot\Delta t-\bar{t}_e^\omega\geqslant-\mathrm{M}(1-\bar{\mu}_e^\omega(t)),\ \forall\ t=0,\ \ldots,T; e\in p^\omega;\omega\in\mathbf{\Omega} \tag{27}$$

Eq. (27) indicates that $\bar{\mu}_e^\omega(t)=1$ if $t\cdot\Delta t>\bar{t}_e^\omega$ (i.e., vehicle ω has passed the stop bar on edge e by time step t) and $\bar{\mu}_e^\omega(t)=0$, otherwise.

3.1.6. No lane changing zone

A vehicle will not change lanes (i.e., $\delta_k^\omega(t+1)=\delta_k^\omega(t)$) when it travels in the link of an edge and is close to the stop bar (i.e., $x_e^\omega(t)\leqslant l_e$) as shown in Fig. 2, which is a common practice in real road networks. This is specified by

$$l_e-x_e^\omega(t+1)\leqslant\mathrm{M}(1-|\delta_k^\omega(t+1)-\delta_k^\omega(t)|),\ \forall\ t=0,\ \ldots,T-1; k\in\mathbf{K}_e; e\in p^\omega;\omega\in\mathbf{\Omega} \tag{28}$$

where l_e is a threshold value. When $x_e^\omega(t+1)<l_e$, vehicle ω will remain in its current lane (i.e., $\delta_k^\omega(t+1)=\delta_k^\omega(t)$). Usually, l_e is set to zero. That means vehicles cannot change lanes in the connectors. A larger l_e can also be set for safety concerns, the same as the

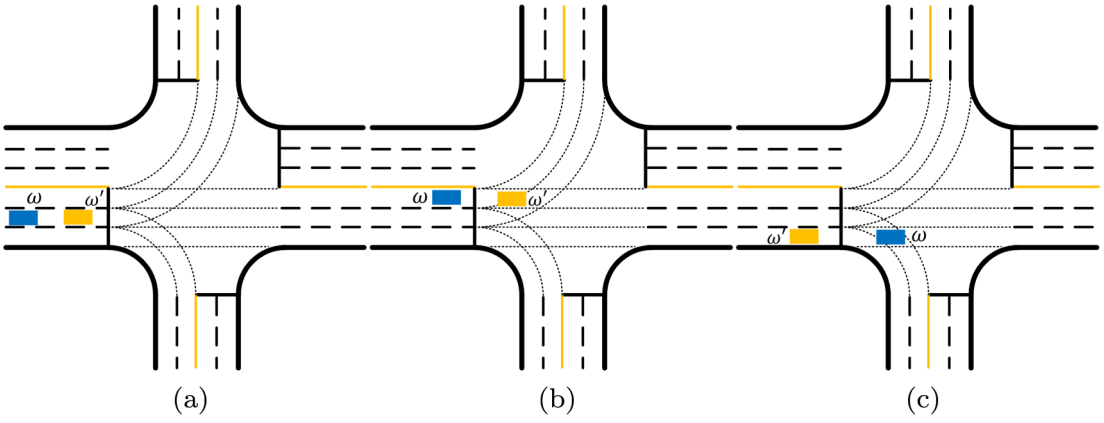

Fig. 7. Vehicles traveling in the same lane: (a) Case 1, (b) Case 2, and (c) Case 3.

solid lane markings close to an intersection in current practice.

3.1.7. Spatial safety gaps between vehicles on one edge

When two vehicles travel in the same lane on one edge, a spatial gap should be applied for safety concerns. The following safety constraints from Newell's car-following model (Newell, 2002) are used:

$$x_e^{\omega}(t) \geqslant x_e^{\omega'}(t - \tau/\Delta t) + d - \mathrm{M}(1 - \zeta_e^{\omega,\omega'}(t) + \rho_e^{\omega,\omega'}(t)),\ \forall\ t = 0,\ ..., T; e \in p^{\omega} \cap p^{\omega'}; \omega' \in \mathbf{\Omega}_{\omega}; \omega \in \mathbf{\Omega} \tag{29}$$

$$x_e^{\omega'}(t) \geqslant x_e^{\omega}(t - \tau/\Delta t) + d - \mathrm{M}(\zeta_e^{\omega,\omega'}(t) + \rho_e^{\omega,\omega'}(t)),\ \forall\ t = 0,\ ..., T; e \in p^{\omega} \cap p^{\omega'}; \omega' \in \mathbf{\Omega}_{\omega}; \omega \in \mathbf{\Omega} \tag{30}$$

where τ and d are the time and space displacement in Newell's car-following model; $\rho_e^{\omega,\omega'}(t)$ is an auxiliary binary variable. When $\rho_e^{\omega,\omega'}(t) = 0$, the constraints of spatial safety gaps are applied, which indicates vehicle ω and vehicle ω' travel in the same lane at time step t. Eq. (29) is effective when $\zeta_e^{\omega,\omega'}(t) = 1$ and Eq. (30) is effective, otherwise. Besides safety, the application of Eqs. (29) and (30) also guarantees the first-in-first-out principle for vehicles in the same lane by the prevention of overtaking in one lane. Note that Δt should be selected properly so that $\tau/\Delta t$ is an integer.

If both vehicle ω and vehicle ω' travel in the same lane in the link of edge e at time step t as shown in Case 1 in Fig. 7, then either Eq. (29) or Eq. (30) should be effective (i.e., $\rho_e^{\omega,\omega'}(t) = 0$), which is guaranteed by

$$\chi_e^{\omega,\omega'}(t) + (2 - \underline{\mu}_e^{\omega}(t) - \underline{\mu}_e^{\omega'}(t) + \bar{\mu}_e^{\omega}(t) + \bar{\mu}_e^{\omega'}(t)) \geqslant \rho_e^{\omega,\omega'}(t)$$
$$\forall\ t = 0, ..., T; e \in p^{\omega} \cap p^{\omega'}; \omega' \in \mathbf{\Omega}_{\omega}; \omega \in \mathbf{\Omega} \tag{31}$$

where $\chi_e^{\omega,\omega'}(t)$ is an auxiliary variable and is defined as

$$\chi_e^{\omega,\omega'}(t) = \sum_{k \in \mathbf{K}_e} |\delta_k^{\omega}(t) - \delta_k^{\omega'}(t)|,\ \forall\ t = 0,\ ..., T; e \in p^{\omega} \cap p^{\omega'}; \omega' \in \mathbf{\Omega}_{\omega}; \omega \in \mathbf{\Omega} \tag{32}$$

Eq. (32) indicates that $\chi_e^{\omega,\omega'}(t) = 0$ if vehicle ω and vehicle ω' are in the same lane on edge e at time step t, and $\chi_e^{\omega,\omega'}(t) = 2$, otherwise. Eqs. (31) and (32) guarantee that $\rho_e^{\omega,\omega'}(t) = 0$ when vehicle ω and vehicle ω' are in the link of the same edge (i.e., $\underline{\mu}_e^{\omega}(t) = \underline{\mu}_e^{\omega'}(t) = 1$ and $\bar{\mu}_e^{\omega}(t) = \bar{\mu}_e^{\omega'}(t) = 0$) and in the same lane (i.e., $\chi_e^{\omega,\omega'}(t) = 0$).

If vehicle ω is in the link of edge e and vehicle ω' is in the connector of edge e (i.e., $\underline{\mu}_e^{\omega}(t) = 1$, $\bar{\mu}_e^{\omega}(t) = 0$, and $\bar{\mu}_e^{\omega'}(t) = 1$) as shown in Case 2 in Fig. 7, then Eq. (29) should be effective (i.e., $\rho_e^{\omega,\omega'}(t) = 0$, $\zeta_e^{\omega,\omega'}(t) = 1$):

$$\chi_e^{\omega,\omega'}(t) + (2 - \underline{\mu}_e^{\omega}(t) - \bar{\mu}_e^{\omega'}(t) + \bar{\mu}_e^{\omega}(t)) \geqslant \rho_e^{\omega,\omega'}(t),\ \forall\ t = 0,\ ..., T; e \in p^{\omega} \cap p^{\omega'}; \omega' \in \mathbf{\Omega}_{\omega}; \omega \in \mathbf{\Omega} \tag{33}$$

$$\chi_e^{\omega,\omega'}(t) + (2 - \underline{\mu}_e^{\omega}(t) - \bar{\mu}_e^{\omega'}(t) + \bar{\mu}_e^{\omega}(t)) \geqslant 1 - \zeta_e^{\omega,\omega'}(t),\ \forall\ t = 0,\ ..., T; e \in p^{\omega} \cap p^{\omega'}; \omega' \in \mathbf{\Omega}_{\omega}; \omega \in \mathbf{\Omega} \tag{34}$$

Similar with Eq. (31), Eqs. (33) and (34) guarantee that $\rho_e^{\omega,\omega'}(t) = 0$ and $\zeta_e^{\omega,\omega'}(t) = 1$, respectively, when $\underline{\mu}_e^{\omega}(t) = \bar{\mu}_e^{\omega'}(t) = 1$, $\bar{\mu}_e^{\omega}(t) = 0$, and $\chi_e^{\omega,\omega'}(t) = 0$.

If vehicle ω' is in the link of edge e and vehicle ω is in the connector of edge e (i.e., $\underline{\mu}_e^{\omega'}(t) = 1$, $\bar{\mu}_e^{\omega'}(t) = 0$, and $\bar{\mu}_e^{\omega}(t) = 1$) as shown in Case 3 in Fig. 7, then Eq. (30) should be effective (i.e., $\rho_e^{\omega,\omega'}(t) = 0$, $\zeta_e^{\omega,\omega'}(t) = 0$):

$$\chi_e^{\omega,\omega'}(t) + (2 - \bar{\mu}_e^{\omega}(t) - \underline{\mu}_e^{\omega'}(t) + \bar{\mu}_e^{\omega'}(t)) \geqslant \rho_e^{\omega,\omega'}(t),\ \forall\ t = 0,\ ..., T; e \in p^{\omega} \cap p^{\omega'}; \omega' \in \mathbf{\Omega}_{\omega}; \omega \in \mathbf{\Omega} \tag{35}$$

$$\chi_e^{\omega,\omega'}(t) + (2 - \bar{\mu}_e^{\omega}(t) - \underline{\mu}_e^{\omega'}(t) + \bar{\mu}_e^{\omega'}(t)) \geqslant \zeta_e^{\omega,\omega'}(t),\ \forall\ t = 0,\ ..., T; e \in p^{\omega} \cap p^{\omega'}; \omega' \in \mathbf{\Omega}_{\omega}; \omega \in \mathbf{\Omega} \tag{36}$$

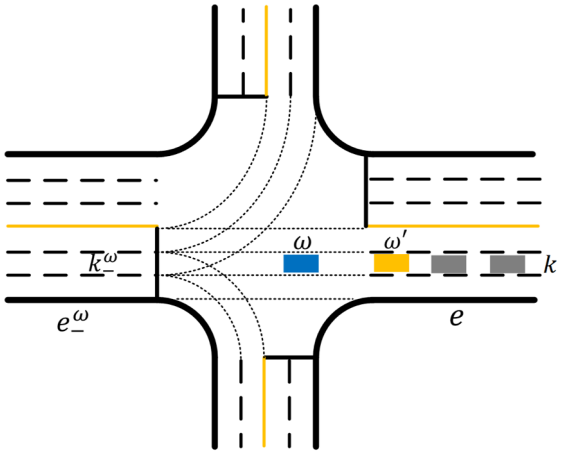

Fig. 8. Spatial safety gaps between vehicles on adjacent edges.

Similar with Eq. (31), Eqs. (35) and (36) guarantee that $\rho_e^{\omega,\omega'}(t) = 0$ and $\zeta_e^{\omega,\omega'}(t) = 0$, respectively, when $\underline{\mu}_e^{\omega'}(t) = \bar{\mu}_e^{\omega}(t) = 1$, $\bar{\mu}_e^{\omega'}(t) = 0$, and $\chi_e^{\omega,\omega'}(t) = 0$.

3.1.8. Temporal safety gaps between vehicles on one edge

When two vehicles consecutively pass the stop bar in the same lane as shown in Case 2 and Case 3 in Fig. 7, a temporal gap between their passing times should be applied. The following safety constraints from Newell's car-following model (Newell, 2002) are used:

$$\bar{t}_e^{\omega} \geqslant \bar{t}_e^{\omega'} + \frac{d}{v_e^{\omega'}} + \tau - \mathrm{M}(1 - \bar{\zeta}_e^{\omega,\omega'} + \chi_e^{\omega,\omega'}(T)),\ \forall\, e \in p^{\omega} \cap p^{\omega'}; \omega' \in \boldsymbol{\Omega}_{\omega}; \omega \in \boldsymbol{\Omega} \tag{37}$$

$$\bar{t}_e^{\omega'} \geqslant \bar{t}_e^{\omega} + \frac{d}{v_e^{\omega}} + \tau - \mathrm{M}(\bar{\zeta}_e^{\omega,\omega'} + \chi_e^{\omega,\omega'}(T)),\ \forall\, e \in p^{\omega} \cap p^{\omega'}; \omega' \in \boldsymbol{\Omega}_{\omega}; \omega \in \boldsymbol{\Omega} \tag{38}$$

where $\chi_e^{\omega,\omega'}(T)$ is defined in the above Eq. (32). $\bar{\zeta}_e^{\omega,\omega'}$ is an introduced binary variable. Eq. (37) is effective when $\bar{\zeta}_e^{\omega,\omega'} = 1$; and Eq. (38) is effective, otherwise. These constraints are used to guarantee the safety between two vehicles with different movements in the connectors (i.e., diverging conflicts).

3.1.9. Spatial safety gaps between vehicles on adjacent edges

When traffic demand is high and intersections along the corridor are close to each other, spillbacks may occur. Assume vehicle ω' is in lane k on edge e and vehicle ω is running from a connector of the preceding edge $\underline{e}^{\omega}$ into lane k. Vehicle ω and vehicle ω' may have a collision due to spillbacks as shown in Fig. 8. To avoid such collision, the following constraints are used:

$$\begin{aligned} &x_{\underline{e}^{\omega}}^{\omega}(t) + l_{\underline{k}^{\omega}}^{\omega} + L_e \geqslant x_e^{\omega'}(t - \tau/\Delta t) + d - \mathrm{M}(2 - \delta_{\underline{k}^{\omega}}^{\omega}(T) - \delta_k^{\omega'}(t) + \tilde{\zeta}_e^{\omega,\omega'}(t)) \\ &\forall\, t = 0, \ldots, T; k \in \mathbf{K}_e; e \in p^{\omega} \cap p^{\omega'}; \omega' \in \boldsymbol{\Omega}_{\omega}; \omega \in \boldsymbol{\Omega} \end{aligned} \tag{39}$$

$$2 - \underline{\mu}_e^{\omega'}(t) - \bar{\mu}_{\underline{e}^{\omega}}^{\omega}(t) + \underline{\mu}_e^{\omega}(t) \geqslant \tilde{\zeta}_e^{\omega,\omega'}(t),\ \forall\, t = 0, \ldots, T; e \in p^{\omega} \cap p^{\omega'}; \omega' \in \boldsymbol{\Omega}_{\omega}; \omega \in \boldsymbol{\Omega} \tag{40}$$

where $\tilde{\zeta}_e^{\omega,\omega'}(t)$ is an auxiliary binary variable. Eq. (40) guarantees that $\tilde{\zeta}_e^{\omega,\omega'}(t) = 0$ if vehicle ω' is on edge e (i.e., $\underline{\mu}_e^{\omega'}(t) = 1$) and vehicle ω is in a connector of the preceding edge $\underline{e}^{\omega}$ (i.e., $\bar{\mu}_{\underline{e}^{\omega}}^{\omega}(t) = 1$ and $\underline{\mu}_e^{\omega}(t) = 0$). $\underline{k}^{\omega}$ is the lane on edge $\underline{e}^{\omega}$ that is connected to lane k on edge e. $l_{\underline{k}^{\omega}}$ is the length of the connector connecting lane $\underline{k}^{\omega}$ and lane k. Eq. (39) guarantees the safety gap between vehicle ω' and vehicle ω similar to Eq. (29). As vehicles travel at constant speeds within the intersection area, they will not travel into the connectors when spillbacks occur.

3.1.10. Collision avoidance within intersection areas

Suppose vehicle ω on edge e and vehicle ω' on edge e' are running toward the same intersection (i.e., $i_e = i_{e'}$) as shown in Fig. 2. To avoid collisions at the conflict point within the intersection area, a clearance time between $\bar{t}_e^{\omega}$ and $\bar{t}_{e'}^{\omega'}$ of vehicle ω and vehicle ω' is applied as shown in Eqs. (41)–(43):

$$\bar{t}_{e'}^{\omega'} - \bar{t}_e^{\omega} \geqslant \pi_{\omega',e'}^{\omega,e} - \mathrm{M}\gamma_{\omega',e'}^{\omega,e},\ \forall\, e \in p^{\omega},\ e' \in p^{\omega'},\ i_e = i_{e'}; \omega,\ \omega' \in \boldsymbol{\Omega} \tag{41}$$

$$\bar{t}_e^{\omega} - \bar{t}_{e'}^{\omega'} \geqslant \pi_{\omega,e}^{\omega',e'} - \mathrm{M}\gamma_{\omega,e}^{\omega',e'},\ \forall\, e \in p^{\omega},\ e' \in p^{\omega'},\ i_e = i_{e'}; \omega,\ \omega' \in \boldsymbol{\Omega} \tag{42}$$

$$\gamma_{\omega',e'}^{\omega,e} + \gamma_{\omega,e}^{\omega',e'} = 1, \forall\, e \in p^{\omega}, e' \in p^{\omega'}, i_e = i_{e'}; \omega, \omega' \in \mathbf{\Omega} \tag{43}$$

where $\gamma_{\omega',e'}^{\omega,e}$ and $\gamma_{\omega,e}^{\omega',e'}$ are auxiliary binary variables. Eq. (41) is effective if $\gamma_{\omega',e'}^{\omega,e} = 0$. Eq. (42) is effective if $\gamma_{\omega,e}^{\omega',e'} = 0$. $\pi_{\omega,e}^{\omega',e'}$ is the clearance time between the departure times from stop bars if vehicle ω' from edge e' follows vehicle ω from edge e to pass their conflict point.

$\pi_{\omega',e'}^{\omega,e}$ is determined by the lanes in which vehicle ω and vehicle ω' pass the stop bars. The two lanes may belong to the same edge (e.g., vehicle ω and vehicle ω_1 in Fig. 2) or different edges (e.g., vehicle ω and vehicle ω_2 in Fig. 2).

$$\begin{aligned} &-\mathrm{M}(2 - \delta_k^{\omega}(T) - \delta_{k'}^{\omega'}(T)) \leqslant \pi_{\omega',e'}^{\omega,e} - \pi_{\omega',k'}^{\omega,k} \leqslant \mathrm{M}(2 - \delta_k^{\omega}(T) - \delta_{k'}^{\omega'}(T)) \\ &\forall\, k \in \mathbf{K}_e^{\omega}, k' \in \mathbf{K}_{e'}^{\omega'}; e \in p^{\omega}, e' \in p^{\omega'}, i_e = i_{e'}; \omega, \omega' \in \mathbf{\Omega} \end{aligned} \tag{44}$$

where $\pi_{\omega',k'}^{\omega,k}$ is determined given the layout of the intersection and is calculated based on the travel time from stop bars to the conflict point and the safety time gap st:

$$\pi_{\omega',k'}^{\omega,k} = tt_{\omega',k'}^{\omega,k} - tt_{\omega,k}^{\omega',k'} + st, \forall\, k \in \mathbf{K}_e^{\omega}, k' \in \mathbf{K}_{e'}^{\omega'}; e \in p^{\omega}, e' \in p^{\omega'}, i_e = i_{e'}; \omega, \omega' \in \mathbf{\Omega} \tag{45}$$

where $tt_{\omega',k'}^{\omega,k}$ is the travel time of vehicle ω from the stop bar to the conflict point if vehicle ω enters the intersection from lane k and vehicle ω' enters the intersection from lane k'. Note that the above constraints should be applied for each point if multiple conflict points exist.

3.2. Objective function

The objective of the optimization model is to minimize total vehicle delay. Vehicle delay is defined as the difference between the actual travel time and the free flow travel time. The actual travel time is calculated as the difference between the times when a vehicle leaves and enters the corridor. The free flow travel time is determined from each vehicle's path. Therefore, minimizing vehicle delay is equivalent to minimizing vehicle's leaving time as the entering time is always a constant. The objective function is formulated as

$$\min \sum_{\omega \in \mathbf{\Omega}} \bar{t}_{p_+^{\omega}}^{\omega} \tag{46}$$

where $\bar{t}_{p_+^{\omega}}^{\omega}$ is the time when vehicle ω leaves its path. However, multiple optimal solutions may exist in terms of total vehicle delay. And the vehicle trajectories of certain solutions are unfavorable. For example, the two trajectories in Fig. 9 have the same delay. But the second trajectory blocks traffic in the middle of the link and thus the first trajectory is preferred. To this end, a secondary objective is added:

$$\min \sum_{\omega \in \mathbf{\Omega}} \sum_{e \in p^{\omega}} \sum_{t=0}^{T} x_e^{\omega}(t) \tag{47}$$

Note that the secondary objective also causes the occurrence of shockwaves at the stop bars. Because the safety constraints in Section 3.1.7 are derived from Newell's car-following model (Newell, 2002), which takes shockwaves into consideration.

To combine Eqs. (46) and (47), the final objective function is shown as

$$\min w_1 \sum_{\omega \in \mathbf{\Omega}} \bar{t}_{p_+^{\omega}}^{\omega} + w_2 \sum_{\omega \in \mathbf{\Omega}} \sum_{e \in p^{\omega}} \sum_{t=0}^{T} x_e^{\omega}(t) \tag{48}$$

where w_1 and w_2 are weighting parameters and $w_1 \gg w_2$ to guarantee the solution quality. Constraints include Eqs. (1)–(45). Eqs. (28)

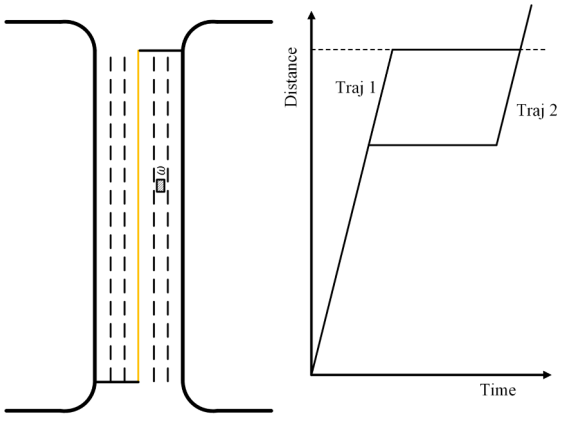

Fig. 9. Illustration of an unrealistic trajectory.

and (32) are in the form of absolute value functions but they can be easily linearized. Due to constraint Eq.(10), constraint Eq. (9) is nonlinear. However, the nonlinearity diminishes with the assumption that the speed of a vehicle within an intersection area is determined by the direction of its movement. Therefore, the proposed model can be solved as an MILP model.

4. Implementation procedure

The challenge of solving the proposed MILP model lies in the large dimensions as well as the inclusion of both continuous and binary variables. Approximately, the number of the variables increases quadratically with the number of the vehicles, linearly with the numbers of the edges and the lanes in the corridor, and the planning horizon length. The number of the constraints varies in a similar way. Further, traffic conditions evolve with new vehicles entering the corridor. The proposed MILP model needs to be solved to update vehicles' planned trajectories considering new vehicle arrivals. Note that the numbers of the vehicles, the edges, and the lanes are fixed in each optimization. Then the planning horizon T becomes a critical parameter in solving the proposed model. The model will be infeasible if T is too small due to constraint Eq. (14). However, a large T brings intensive computational burden. An algorithm is designed to adjust T adaptively and is embedded in the implementation procedure of the proposed model with varying traffic conditions:

Step 0: Initialize planning horizon $T = T_0$ and the simulation time step $t = 0$.
Step 1: Collect information from all the vehicles in the corridor at the current time step t.
Step 2: Solve the MILP model.
Step 3: If there are no feasible solutions, then $T = T + 2\Delta T$, where ΔT is the step length for adjusting T. Go to **Step 2**. Otherwise, get the solutions $\bar{t}^{\omega}_{p^+_{\omega}}$ of each vehicle and go to the next step.
Step 4: Update $T = \max\left(\left\lceil \frac{\max_{\omega\in\Omega}\bar{t}^{\omega}_{p^+_{\omega}}}{\Delta T}\right\rceil, T - \Delta T\right)$, where $\lceil\cdot\rceil$ is the ceiling function.
Step 5: Update $t = t + 1$ and go to **Step 1**.

5. Numerical studies

5.1. Experiment design

To explore the benefits of the proposed cooperative trajectory optimization framework, this study employs an example corridor consisting of four intersections, similar to the one used by Liu and Chang (2011), as shown in Fig. 1. The spacing between adjacent intersections along the corridor is 120 m. The layout of each intersection is given in Fig. 2. There is no specified lane allocation at the intersections. Each ingress lane can be used for left-turning, through, and right-turning traffic if such connectors exist. As the number of ingress lanes on the main road is greater than that of ingress lanes on the downstream side road, not all movements are allowed in some of the ingress lanes as shown in Fig. 2.

There are 10 demand entries (A–J) and four volume levels (low, medium, high, and extremely high) designed to test the performance of the proposed model. The demand generated at each O/D is shown in Table 2. The v/c ratio in Table 2 is the average value of the critical intersection volume-to-capacity ratios (Transportation Research Board (TRB), 2010) of all intersections, which is defined as the sum of the critical v/c ratio of each phase.The turning fractions for all intersection approaches are set to be 30% left-turning, 60% through, and 10% right-turning. The design speed in a connector is 12 m/s for left-turning vehicles, 15 m/s for through vehicles, and 8 m/s for right-turning vehicles. Other main parameters are summarized in Table 3.

It is noted that the algorithms for planning vehicle trajectories in the literature can hardly be applied to the corridor level vehicle trajectory control problem. Because these algorithms did not take into consideration the interactions and coordination between vehicle trajectories at the microscopic level, which is the key to the proposed planning framework. Further, most of the intersection-level control methods focused on the optimization of longitudinal vehicle trajectories but did not take mandatory lane changing into consideration (e.g., Xu et al. (2018) and Yu et al. (2018)). However, such mandatory lane changing may not be overlooked for a vehicle traveling in a corridor. The widely used adaptive signal control systems such as Sydney Coordinated Adaptive Traffic System (ACATS) and Split Cycle Offset Optimisation Technique (SCOOT) can hardly be applied neither because of the difficulty in applying their control mechanisms. However, Tian et al. (2011) found that no significant improvement on arterial progression was achieved

Table 2
Demand scenarios for model evaluation.

Demand scenario	v/c ratio	Demand entries (in vph)									
		A	B	C	D	E	F	G	H	I	J
Low	0.4	600	300	200	300	200	600	200	300	200	300
Medium	0.8	1200	600	400	600	400	1200	400	600	400	600
High	1.2	1800	900	600	900	600	1800	600	900	600	900
Extremely High	1.6	2400	1200	800	1200	800	2400	800	1200	800	1200

Table 3
Main parameters.

Parameter	Value	Parameter	Value	Parameter	Value
Δt	0.5 s	T_0	50	ΔT	4
L_e	120 m	l_e	10 m	$\bar{v}_e^{\omega}$	15 m/s
st	1 s	d	6 m	τ	0.5 s
w_1	400	w_2	1		

with SCATS over conventional coordinated signal plans under normal traffic condition. Therefore, only coordinated fixed-time control is applied as the benchmark, in which case the lane allocation is shown in Fig. 10. Coordinated fixed-time control is expected to achieve the best performance when the intersections are equally spaced. The timing plans are optimized by Synchro 7 (Husch and Albeck, 2006) in each demand scenario with the objective of minimizing delay.

The control algorithm is written in C#. The proposed MILP model is solved using Gurobi 7.0.0 (Gurobi Optimization, Inc., 2016). The optimization model is executed each time when new vehicles are generated at the origins. A time limit of 40 min is set. The solver will return a sub-optimal solution to proceed the simulation when the solving time exceeds the limit. This frequency when a sub-optimal solution is taken increases with rising demand. Only sub-optimal solutions are produced at high and extremely high demand levels. The quality of the sub-optimal solutions depends on the solver and may vary from run to run because of the applied heuristic algorithms in the solver. The simulation is conducted in SUMO (Simulation of Urban Mobility) (Krajzewicz et al., 2012) on a desktop with an Intel 3.6 GHz CPU with 16 GB memory. The default lane-changing model in SUMO, LC2013 (Erdmann, 2015), is used for the benchmark cases. Note that the acceleration/deceleration rates are set as infinity in SUMO so that vehicles can also change speeds and lanes instantaneously in the benchmark cases for fair comparison. Five random seeds are used in the simulation for each demand scenario considering stochastic vehicle arrivals. Each simulation run is 1800 s with a warm-up period of 150 s (Simulation Video).

5.2. Results and discussion

To compare the performance between the coordinated fixed-time control and the proposed CAV-based control, vehicle delay and throughput are used as performance measures. The delay of a vehicle is calculated as the difference between the actual travel time and the free-flow travel time on its path. Therefore, only the delays of the vehicles that have left the corridor are counted. The simulation results are shown in Fig. 11. The details of vehicle delay are shown in Table 4. Note that the v/c ratio in Fig. 11 is an average value. It does not mean all intersections are over-saturated when this value is greater than one. But it helps indicate the overall demand level.

Fig. 11(a) shows that the delays increase with demand when the coordinated fixed-time control and the CAV-based control are applied. The delay under the fixed-time control increases gradually when the demand rises from a low level (v/c = 0.4) to a medium level (v/c = 0.8). However, it increases dramatically when the demand increases to a high level (v/c = 1.2) and an extremely high level (v/c = 1.6), which is consistent with previous studies (Webster, 1958). In comparison, the proposed CAV-based control generates significantly lower delay at all demand levels. The detailed delay values are given in Table 4. Both the average delay and the standard deviation under the CAV-based control are remarkably lower than those under the fixed-time control. It is further observed that the CAV-based control has a better ability to accommodate high demand. For example, the delay under the CAV-based control only increases by ~0.45 time from the low level to the medium level and by ~2.55 times to the extremely high level while the delay under the fixed-time control increases by ~0.23 and ~3.33 times, respectively. The reason is the improved capacity of the corridor

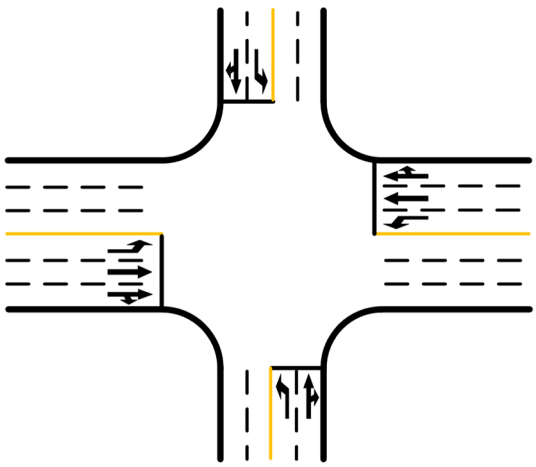

Fig. 10. Lane allocation at each intersection for fixed-time signal control.

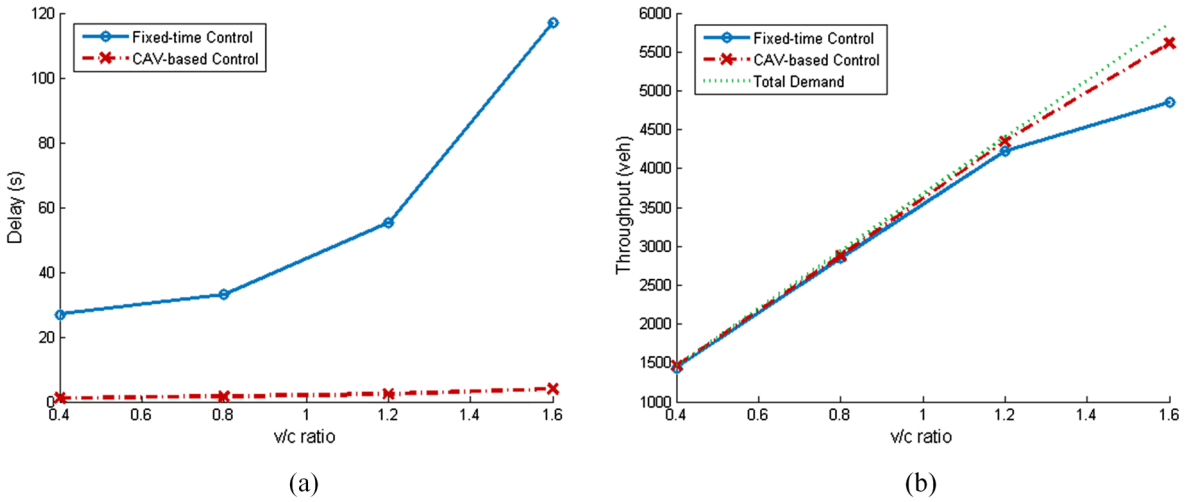

Fig. 11. Simulation results: (a) average vehicle delay, and (b) throughput.

Table 4
Average delay and standard deviation (s).

Delay	Demand Scenarios			
(Standard Deviation)	Low	Medium	High	Extremely High
Coordinated fixed-time Control	27.0 (21.6)	33.1 (24.9)	55.1 (38.6)	116.9 (110.2)
CAV-based Control	1.1 (0.7)	1.6 (1.2)	2.4 (2.0)	3.9 (3.3)

under the CAV-based control as shown in Fig. 11(b). Under the fixed-time control, the vehicle throughput cannot catch up with the total demand when the v/c ratio is greater than 1.2. The slope of the throughput becomes flat when the v/c ratio is 1.6. This is an indication that the intersection capacity is reached. In contrast, the throughput matches the demand well under the CAV-based control even under very high v/c ratios, which means that the demand is still below the capacity. The results show that the CAV-based control improves the intersection capacity significantly. Note that Fig. 11 also indicates the proposed model outperforms the benchmark method to a great extent even when sub-optimal solutions are taken at high demand levels.

The advantages of the CAV-based control over the coordinated fixed-time control come from four major factors:

- No specified lane allocation in ingress lanes. One vehicle can use any ingress lane to pass through an intersection, which enlarges the solution space for vehicle trajectory planning.
- “Signal-free” vehicle management at intersections. Conflicts are avoided based on the individual vehicle level. This noticeably reduces the waste of intersection capacity, especially, under fluctuating traffic flows compared with the fixed-time control.
- Trajectory optimization for one vehicle along its path. The driving behaviors of one vehicle are optimized to reduce its travel time. Specifically, its longitudinal location along its path and its lateral lane choice at each time step are planned jointly.
- Trajectory coordination for vehicles in the corridor. The trajectories of all vehicles in the corridor are coordinated in one unified framework for system optimality in terms of vehicle delay. It is closer to the maximum benefits.

However, it is also noted that the major disadvantage of the proposed centralized control approach is computational challenges, especially, when the vehicle number is large. The computational burden may discourage the application of the centralized control even under the fully CAV environment in the future. There may be several solutions:

- The advances in computational technologies such as quantum computers (IBM News room, 2016) may significantly improve the computational efficiency in the future when the fully CAV environment is realized.
- Following the philosophy of previous studies (Timotheou et al., 2015), cutting-edge distributed solution algorithms may be applied to the centralized optimization problem, e.g., the Alternating Direction Method of Multipliers (ADMM) (Boyd et al., 2011). We leave this for future research.
- The proposed model may only optimize the trajectories of newly arrived vehicles and the planned trajectories of existing vehicles are taken into consideration in constraints for safety concerns. In this way, the number of decision variables is significantly reduced at the cost of system optimality.

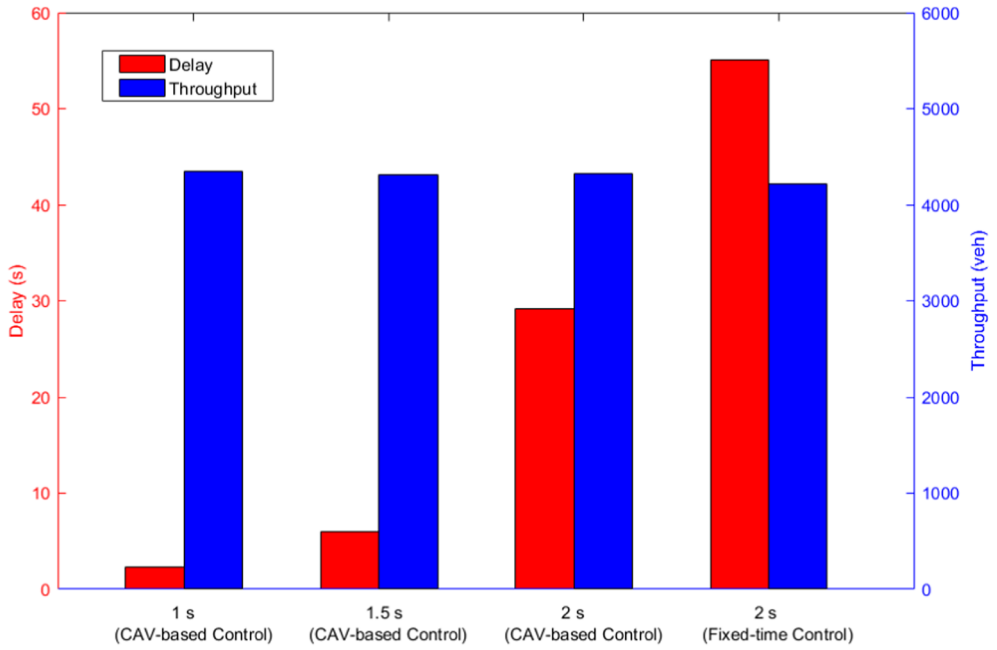

Fig. 12. Impacts of safety time gaps within intersection areas.

5.3. Impacts of safety time gaps within intersection areas

The most noticeable feature of the traffic management in the fully CAV environment is the removal of physical signals at intersections. Collision avoidance is considered at the individual vehicle level between conflicting vehicles rather than at the aggregated level between conflicting traffic flows (i.e., signal phases). The most important parameter is, therefore, the safety time gap *st* in constraints (41)–(45). Intuitively, smaller safety gaps result in higher intersection capacity. To investigate the impacts of the safety gap *st*, the proposed CAV-based control (with $st = 1$ s, 1.5 s, and 2 s) and the coordinated fixed-time control (with the all-red time of 2 s) are compared at the high demand level (v/c = 1.2). The delay and throughput are shown in Fig. 12.

The delay rises significantly under the CAV-based control when the safety time gap increases from 1 s to 2 s. Although the increase of the safety gap is only 0.5 s at each time, the delay increases by more than 100%. Further, the delay under the CAV-based control is still significantly lower than that under the coordinated fixed-time control when the safety gap of the CAV-based control and the all-red clearance time of the fixed-time control are equal (i.e., 2 s). These observations indicate that the "signal-free" CAV-based control is a promising direction for intersection management. However, the throughput reduction is insignificant with a longer safety gap, due to the increased intersection capacity that prevents the intersection becoming oversaturated. This also account for the observation that the throughput under the CAV-based control and the fixed-time control are both slightly below the demand in Fig. 11(b) even though the v/c ratio is 1.2.

6. Conclusions and recommendations

This study proposes an MILP model to cooperatively optimize the trajectories of vehicles along a "signal-free" corridor in the fully CAV environment. The car-following and the lane-changing behaviors of each individual vehicle along the whole path are optimized jointly. The trajectories of all vehicles in the corridor are coordinated in one unified framework for system optimality in terms of total vehicle delay. The interactions of vehicle trajectories are modeled explicitly at the microscopic level considering both safety and efficiency. All movements including left-turning, through, and right-turning are considered at each intersection. One significant improvement of the proposed work over previous studies is that lane allocation is not specified for each lane, which means every lane can be used for all vehicle movements. Vehicles are managed at the individual level without physical signals. In the implementation procedure, the planning horizon is adaptively adjusted to make a balance between the feasibility of the MILP model and the computational efficiency. Numerical studies show that the proposed CAV-based control outperforms coordinated fixed-time control significantly in terms of both vehicle delay and throughput. The analysis of the impacts of the safety time gap for collision avoidance within intersection areas indicates that the proposed model can greatly increase the intersection capacity.

This study assumes a fully CAV environment. However, regular vehicles and CAVs will coexist in the near future. It is worthwhile to extend the proposed model to the mixed traffic environment. To this end, additional considerations are needed: 1) Prediction of the trajectories of regular vehicles (i.e., non-CAVs) to estimate vehicle delays and avoid collisions; 2) Inclusion of lane allocation and signal optimization to cater to regular vehicles; and 3) CAV trajectory planning at the strategic level because CAVs may not be able to exactly follow the planned trajectories under the mixed traffic environment. Considering communication delays and detection issues,

robust optimization of CAV trajectories is another research direction. For example, the receding horizon control (RHC) method in Kuwata and How (2011) can be explored for robust trajectory optimization. In addition, the computational burden is heavy, especially at higher demand levels. It is of interest to develop an efficient algorithm for the proposed MILP model. Vehicle paths are assumed fixed in this study. It is planned to extend the proposed model to a network level where vehicle paths can be optimized as well.

Acknowledgements

This research was funded by the U.S. Department of Transportation (USDOT) Center for Connected and Automated Transportation (CCAT) at University of Michigan, Shanghai Sailing Program (No. 19YF1451600), the National Natural Science Foundation of China (No. 51722809 and No. 61773293), and the Fok Ying Tong Education Foundation (No. 151076). The views presented in this paper are those of the authors alone.

References

Allsop, R.E., 1976. SIGCAP: A computer program for assessing the traffic capacity of signal-controlled road junctions. Traffic Eng. Control 17, 338–341.
Alonso, J., Milanés, V., Pérez, J., Onieva, E., González, C., de Pedro, T., 2011. Autonomous vehicle control systems for safe crossroads. Transport. Res. Part C: Emerg. Technol. 19, 1095–1110. https://doi.org/10.1016/j.trc.2011.06.002. URL. http://www.sciencedirect.com/science/article/pii/S0968090X11000921.
Au, T.-C., Stone, P., 2010. Motion planning algorithms for autonomous intersection management. In: Proceedings of the 1st AAAI Conference on Bridging the Gap Between Task and Motion Planning AAAIWS'10-01. AAAI Press, pp. 2–9. URL. http://dl.acm.org/citation.cfm?id=2908515.2908516.
Boyd, S., Parikh, N., Chu, E., Peleato, B., Eckstein, J., 2011. Distributed optimization and statistical learning via the alternating direction method of multipliers. Found. Trends® Mach. Learn. 3, 1–122. https://doi.org/10.1561/2200000016.
Carlino, D., Boyles, S.D., Stone, P., 2013. Auction-based autonomous intersection management. In: 16th International IEEE Conference on Intelligent Transportation Systems (ITSC 2013), pp. 529–534. https://doi.org/10.1109/ITSC.2013.672828.
Dresner, K., Stone, P., 2008. A multiagent approach to autonomous intersection management. J. Artif. Intell. Res. 31, 591–656.
Erdmann, J., 2015. SUMO's lane-changing model. In: Behrisch, M., Weber, M. (Eds.), Modeling Mobility with Open Data. Springer International Publishing, Cham, pp. 105–123.
Feng, Y., Head, K.L., Khoshmagham, S., Zamanipour, M., 2015. A real-time adaptive signal control in a connected vehicle environment. Transport. Res. Part C: Emerg. Technol. 55, 460–473. https://doi.org/10.1016/j.trc.2015.01.007. URL. http://www.sciencedirect.com/science/article/pii/S0968090X15000091.
Feng, Y., Yu, C., Liu, H.X., 2018. Spatial and temporal intersection control in a connected and automated vehicle environment. Transport. Res. Part C: Emerg. Technol. 89, 364–383.
Giridhar, A., Kumar, P.R., 2006. Scheduling automated traffic on a network of roads. IEEE Trans. Veh. Technol. 55, 1467–1474. https://doi.org/10.1109/TVT.2006.877472. URL. http://ieeexplore.ieee.org/ielx5/25/35959/01703949.pdf?tp=&arnumber=1703949&isnumber=35959.
Gradinescu, V., Gorgorin, C., Diaconescu, R., Cristea, V., Iftode, L., 2007. Adaptive traffic lights using car-to-car communication. In: 2007 IEEE 65th Vehicular Technology Conference - VTC2007-Spring, pp. 21–25. https://doi.org/10.1109/VETECS.2007.17.
Guo, Q., Li, L., Ban, X.J., 2019a. Urban traffic signal control with connected and automated vehicles: A survey. Transport. Res. Part C: Emerg. Technol. 101, 313–334. https://doi.org/10.1016/j.trc.2019.01.026. URL. http://www.sciencedirect.com/science/article/pii/S0968090X18311641.
Guo, Y., Ma, J., Xiong, C., Li, X., Zhou, F., Hao, W., 2019b. Joint optimization of vehicle trajectories and intersection controllers with connected automated vehicles: Combined dynamic programming and shooting heuristic approach. Transport. Res. Part C: Emerg. Technol. 98, 54–72. https://doi.org/10.1016/j.trc.2018.11.010. URL. http://www.sciencedirect.com/science/article/pii/S0968090X18303279.
Gurobi Optimization, Inc., 2016. Gurobi optimizer reference manual. URL: http://www.gurobi.com/.
Han, K., Gayah, V.V., 2015. Continuum signalized junction model for dynamic traffic networks: Offset, spillback, and multiple signal phases. Transport. Res. Part B: Methodol. 77, 213–239. https://doi.org/10.1016/j.trb.2015.03.005. URL. http://www.sciencedirect.com/science/article/pii/S019126151500048X.
Han, K., Gayah, V.V., Piccoli, B., Friesz, T.L., Yao, T., 2014. On the continuum approximation of the on-and-off signal control on dynamic traffic networks. Transport. Res. Part B: Methodol. 61, 73–97. https://doi.org/10.1016/j.trb.2014.01.001. URL. http://www.sciencedirect.com/science/article/pii/S0191261514000022.
Hausknecht, M., Au, T.C., Stone, P., 2011. Autonomous intersection management: multi-intersection optimization. In: 2011 IEEE/RSJ International Conference on Intelligent Robots and Systems, pp. 4581–4586. https://doi.org/10.1109/IROS.2011.6094668.
He, Q., Head, K.L., Ding, J., 2012. PAMSCOD: Platoon-based arterial multi-modal signal control with online data. Transport. Res. Part C: Emerg. Technol. 20, 164–184. https://doi.org/10.1016/j.trc.2011.05.007. URL. http://www.sciencedirect.com/science/article/pii/S0968090X11000775.
He, X., Liu, H.X., Liu, X., 2015. Optimal vehicle speed trajectory on a signalized arterial with consideration of queue. Transport. Res. Part C: Emerg. Technol. 61, 106–120. https://doi.org/10.1016/j.trc.2015.11.001. URL. http://www.sciencedirect.com/science/article/pii/S0968090X15003800.
Heydecker, B.G., 1992. Sequencing of Traffic Signals. Mathematics in Transport Planning and Control. Clarendon Press, Oxford.
Husch, D., Albeck, J., 2006. Synchro Studio 7 User Guide, vol. 41 Trafficware Ltd, Sugar Land, TX, USA.
IBM News room, 2016. IBM makes quantum computing available on IBM cloud to accelerate innovation. [ONLINE] Available at: https://www-03.ibm.com/press/us/en/pressrelease/49661.wss [Accessed 5 June 2017].
Ilgin Guler, S., Menendez, M., Meier, L., 2014. Using connected vehicle technology to improve the efficiency of intersections. Transport. Res. Part C: Emerg. Technol. 46, 121–131. https://doi.org/10.1016/j.trc.2014.05.008. URL. http://www.sciencedirect.com/science/article/pii/S0968090X14001211.
Kamal, M.A.S., Mukai, M., Murata, J., Kawabe, T., 2013. Model predictive control of vehicles on urban roads for improved fuel economy. IEEE Trans. Control Syst. Technol. 21, 831–841. https://doi.org/10.1109/TCST.2012.2198478.
Kamalanathsharma, R.K., Rakha, H.A., 2013. Multi-stage dynamic programming algorithm for eco-speed control at traffic signalized intersections. In: 16th International IEEE Conference on Intelligent Transportation Systems (ITSC 2013), pp. 2094–2099. https://doi.org/10.1109/ITSC.2013.672853.
Krajzewicz, D., Erdmann, J., Behrisch, M., Bieker, L., 2012. Recent development and applications of SUMO - Simulation of Urban MObility. Int. J. Adv. Syst. Measur. 5, 128–138.
Kuwata, Y., How, J.P., 2011. Cooperative distributed robust trajectory optimization using receding horizon MILP. IEEE Trans. Control Syst. Technol. 19, 423–431.
Lee, J., Park, B., 2012. Development and evaluation of a cooperative vehicle intersection control algorithm under the connected vehicles environment. IEEE Trans. Intell. Transp. Syst. 13, 81–90.
Levin, M.W., Fritz, H., Boyles, S.D., 2017. On optimizing reservation-based intersection controls. IEEE Trans. Intell. Transp. Syst. 18, 505–515. https://doi.org/10.1109/TITS.2016.2574948. URL. http://ieeexplore.ieee.org/ielx7/6979/7865878/07514999.pdf?tp=&arnumber=7514999&isnumber=7865878.
Li, Z., Chitturi, M., Zheng, D., Bill, A., Noyce, D., 2013. Modeling reservation-based autonomous intersection control in VISSIM. Transport. Res. Rec.: J. Transport. Res. Board 2381, 81–90. https://doi.org/10.3141/2381-10.
Li, Z., Elefteriadou, L., Ranka, S., 2014. Signal control optimization for automated vehicles at isolated signalized intersections. Transport. Res. Part C: Emerg. Technol. 49, 1–18. https://doi.org/10.1016/j.trc.2014.10.001. URL. http://www.sciencedirect.com/science/article/pii/S0968090X14002939.
Li, Z., Wu, Q., Yu, H., Chen, C., Zhang, G., Tian, Z.Z., Prevedouros, P.D., 2019. Temporal-spatial dimension extension-based intersection control formulation for connected and autonomous vehicle systems. Transport. Res. Part C: Emerg. Technol. 104, 234–248. https://doi.org/10.1016/j.trc.2019.05.003. URL. http://www.sciencedirect.com/science/article/pii/S0968090X18305436.

Liang, X.J., Guler, S.I., Gayah, V.V., 2018. Signal timing optimization with connected vehicle technology: platooning to improve computational efficiency. Transp. Res. Rec. 0, 0. https://doi.org/10.1177/0361198118786842.
Little, J.D.C., Kelson, M.D., Gartner, N.M., 1981. MAXBAND: A program for setting signals on arteries and triangular networks. Transport. Res. Rec.: J. Transport. Res. Board 795, 40–46.
Liu, R., Smith, M., 2015. Route choice and traffic signal control: A study of the stability and instability of a new dynamical model of route choice and traffic signal control. Transport. Res. Part B: Methodol. 77, 123–145. https://doi.org/10.1016/j.trb.2015.03.012. URL. http://www.sciencedirect.com/science/article/pii/S0191261515000557.
Liu, Y., Chang, G.-L., 2011. An arterial signal optimization model for intersections experiencing queue spillback and lane blockage. Transport. Res. Part C: Emerg. Technol. 19, 130–144. https://doi.org/10.1016/j.trc.2010.04.005.
Memoli, S., Cantarella, G.E., de Luca, S., Pace, R.D., 2017. Network signal setting design with stage sequence optimisation. Transport. Res. Part B: Methodol. 100, 20–42. https://doi.org/10.1016/j.trb.2017.01.013. URL. http://www.sciencedirect.com/science/article/pii/S0191261516302363.
Mirheli, A., Tajalli, M., Hajibabai, L., Hajbabaie, A., 2019. A consensus-based distributed trajectory control in a signal-free intersection. Transport. Res. Part C: Emerg. Technol. 100, 161–176. https://doi.org/10.1016/j.trc.2019.01.004. URL. http://www.sciencedirect.com/science/article/pii/S0968090X18311343.
Miyatake, M., Kuriyama, M., Takeda, Y., 2011. Theoretical study on eco-driving technique for an electric vehicle considering traffic signals. In: 2011 IEEE Ninth International Conference on Power Electronics and Drive Systems, pp. 733–738. https://doi.org/10.1109/PEDS.2011.6147334.
Newell, G.F., 2002. A simplified car-following theory: a lower order model. Transport. Res. Part B: Methodol. 36, 195–205. https://doi.org/10.1016/S0191-2615(00)00044-8. URL. http://www.sciencedirect.com/science/article/pii/S0191261500000448.
Papageorgiou, M., Diakaki, C., Dinopoulou, V., Kotsialos, A., Wang, Y., 2003. Review of road traffic control strategies. Proc. IEEE 91, 2043–2067. https://doi.org/10.1109/JPROC.2003.819610.
Tachet, R., Santi, P., Sobolevsky, S., Reyes-Castro, L.I., Frazzoli, E., Helbing, D., Ratti, C., 2016. Revisiting street intersections using slot-based systems. PLoS ONE 11https://doi.org/10.1371/journal.pone.0149607. e0149607.
Tian, Z., Ohene, F., Hu, P., 2011. Arterial performance evaluation on an adaptive traffic sgnal control system. Procedia - Social Behav. Sci. 16, 230–239. https://doi.org/10.1016/j.sbspro.2011.04.445. URL. http://www.sciencedirect.com/science/article/pii/S1877042811009918 6th International Symposium on Highway Capacity and Quality of Service.
Timotheou, S., Panayiotou, C.G., Polycarpou, M.M., 2015. Distributed traffic signal control using the cell transmission model via the alternating direction method of multipliers. IEEE Trans. Intell. Transp. Syst. 16, 919–933. https://doi.org/10.1109/TITS.2014.2347300.
Transportation Research Board (TRB), 2010. HCM 2010: Highway Capacity Manual. Transportation Research Board, Washington, D.C.
Ubiergo, G.A., Jin, W.-L., 2016. Mobility and environment improvement of signalized networks through Vehicle-to-Infrastructure (V2I) communications. Transport. Res. Part C: Emerg. Technol. 68, 70–82. https://doi.org/10.1016/j.trc.2016.03.010. URL. http://www.sciencedirect.com/science/article/pii/S0968090X16300031.
Wan, N., Vahidi, A., Luckow, A., 2016. Optimal speed advisory for connected vehicles in arterial roads and the impact on mixed traffic. Transport. Res. Part C: Emerg. Technol. 69, 548–563. https://doi.org/10.1016/j.trc.2016.01.011. URL. http://www.sciencedirect.com/science/article/pii/S0968090X16000292.
Wang, M., Daamen, W., Hoogendoorn, S.P., Van Arem, B., 2014a. Rolling horizon control framework for driver assistance systems. Part I: Mathematical formulation and non-cooperative systems. Transport. Res. Part C: Emerg. Technol. 40, 271–289. https://doi.org/10.1016/j.trc.2013.11.023. URL. http://www.sciencedirect.com/science/article/pii/S0968090X13002593.
Wang, M., Daamen, W., Hoogendoorn, S.P., Van Arem, B., 2014b. Rolling horizon control framework for driver assistance systems. Part II: Cooperative sensing and cooperative control. Transport. Res. Part C: Emerg. Technol. 40, 290–311. https://doi.org/10.1016/j.trc.2013.11.024. URL. http://www.sciencedirect.com/science/article/pii/S0968090X13002611.
Webster, F.V., 1958. Traffic signal settings volume 39 of Road Research Technical Paper. Her Majesty's Stationery Office, London, England.
Xu, B., Li, S.E., Bian, Y., Li, S., Ban, X.J., Wang, J., Li, K., 2018. Distributed conflict-free cooperation for multiple connected vehicles at unsignalized intersections. Transport. Res. Part C: Emerg. Technol. 93, 322–334. https://doi.org/10.1016/j.trc.2018.06.004. URL. http://www.sciencedirect.com/science/article/pii/S0968090X18308246.
Yang, K., Menendez, M., Guler, S.I., 2018. Implementing transit signal priority in a connected vehicle environment with and without bus stops. Transport. B: Transport Dyn. 0, 1–23. https://doi.org/10.1080/21680566.2018.1434019.
Yang, K., Zheng, N., Menendez, M., 2017. Multi-scale perimeter control approach in a connected-vehicle environment. Transport. Res. Procedia 23, 101–120. https://doi.org/10.1016/j.trpro.2017.05.007. URL. http://www.sciencedirect.com/science/article/pii/S2352146517302843 Papers Selected for the 22nd International Symposium on Transportation and Traffic Theory Chicago, Illinois, USA, 24-26 July, 2017.
Yu, C., Feng, Y., Liu, H.X., Ma, W., Yang, X., 2018. Integrated optimization of traffic signals and vehicle trajectories for isolated urban intersections. Transport. Res. Part B: Methodol. 112, 89–112.
Zhu, F., Ukkusuri, S.V., 2015. A linear programming formulation for autonomous intersection control within a dynamic traffic assignment and connected vehicle environment. Transport. Res. Part C: Emerg. Technol. 55, 363–378. https://doi.org/10.1016/j.trc.2015.01.006. URL. http://www.sciencedirect.com/science/article/pii/S0968090X1500008X.
Zohdy, I.H., Rakha, H.A., 2016. Intersection management via vehicle connectivity: the intersection cooperative adaptive cruise control system concept. J. Intell. Transport. Syst. 20, 17–32. https://doi.org/10.1080/15472450.2014.889918.